Mesh sensitivity of vertical axis turbine wakes for farm simulations

P.-L. Delafin[a], S. Guillou[b], J. Sommeria[a], T. Maître[a]

a. Univ. Grenoble Alpes, CNRS, Grenoble INP, LEGI, 38000 Grenoble, France
pierre-luc.delafin@grenoble-inp.fr
b. Laboratoire Universitaire des Sciences Appliquées de Cherbourg, UNICAEN, 60 rue Max-Pol Fouchet, 50130 Cherbourg-en-Cotentin, France

Résumé :

Ce travail utilise des simulations URANS 2D d'une turbine à axe vertical isolée (turbine seule, non confinée) afin d'étudier l'effet de la résolution du maillage sur la prédiction du sillage. Quatre raffinements de maillages sont testés et la comparaison des profils de vitesse axiale et d'énergie cinétique turbulente moyennées permet de recommander, dans le sillage, l'emploi de mailles de dimensions $\Delta x = \Delta y = D/20$, avec D le diamètre de la turbine. La comparaison des profils de vitesse et d'énergie cinétique turbulente jusqu'à 12 diamètres en aval avec des données expérimentales permet de montrer les limitations de la modélisation 2D pour des applications de type "fermes de turbines".

Abstract :

This work uses 2D URANS simulations of an isolated vertical axis turbine (one single turbine with a very low blockage ratio) in order to study the mesh sensitivity of the wake prediction. To that end, four grids are tested and the comparison of the average velocity and turbulence kinetic energy profiles shows that it is better to use a minimum refinement $\Delta x = \Delta y = D/20$, with D the turbine diameter. Furthermore, the comparison of velocity and turbulence kinetic energy profiles up to 12 diameters downstream the turbine with experimental data shows the limitations of a 2D model if farms applications are considered.

Keywords: Vertical axis turbines, Tidal turbines, CFD, Wakes, Tidal farm.

1 Introduction

The wind turbine industry is one of the fastest growing renewable energy industries and wind farms are now being built offshore with projects of operating floating turbines. Vertical axis turbines (VAT) present some advantages over the classical horizontal axis turbines when considering floating applications. They do not need any yawing system since they are insensitive to the wind direction and the drive train and generator may be placed close to the sea surface which makes maintenance easier. Also, the lower altitude of the drive train components compared to a horizontal axis configuration increases the stability of the turbine which in turn reduces the cost of the floating platform. These advantages are also valid for tidal or river flows applications.

Within a farm, turbines interact with each other and it is therefore important to have a good understanding of the wake and its recovery. The wake of horizontal axis turbines has already been studied a lot, both experimentally and numerically. However, the wake of VAT has started to be studied more recently. Especially, studies covering both near and far wakes have been carried out recently [1, 2, 3]. Simulations of VAT generally base their grid convergence study on the variation of the coefficient of power of the rotor. When focusing on the turbine wake, this criteria is not sufficient because the grid resolution may change significantly between the rotor region and the far wake region. Furthermore, the far wake needs more time than the coefficient of power of the turbine to reach a stationary (or periodic) state.

In this work, we use 2D URANS simulations to study the sensitivity of a VAT wake to the mesh resolution. Both near and far wakes are addressed (up to 12 diameters downstream the rotor) and simulations results are compared to experimental data recently published [2]. The aim is to provide guidelines regarding the minimum mesh resolution to use for an efficient wake description and to give information about the level of accuracy that can be expected from a 2D simulation, when compared to results of an actual 3D turbine.

2 Methods

2.1 Turbine and operating conditions

The turbine used in this study is the same as the one tested in [2] (Fig. 1a). It is a 3-bladed vertical axis turbine with straight blades. The turbine diameter is $D = 0.175$ m and the blade span is $l = 0.175$ m which gives a rotor swept area $S = 0.0306$ m^2. Blades are NACA 0018 sections whose mean lines are projected on the circle along which they travel (Fig. 1b). The chord length $c = 0.032$ m is constant over the span. The turbine solidity, as defined in [1], is therefore $\sigma = \frac{nc}{\pi D} = 0.175$, with n the number of blades.

The freestream water speed is $U_\infty = 2.3$ m/s as in the experiments and water has the standard characteristics: $\rho = 998.2$ kg/m^3 and $\nu = 1.0048 \times 10^{-6}$ m^2/s. For most of the work presented here, the turbine is operating at a tip speed ratio ($TSR = \omega R/U_\infty$, with ω the turbine rotational speed and R the turbine radius) equal to 2 which corresponds to its optimal operating condition. The Reynolds number based on the relative flow speed (W) and the chord length (c), $Re_c = \frac{Wc}{\nu}$, varies between 7×10^4 and 2.2×10^5 over a revolution.

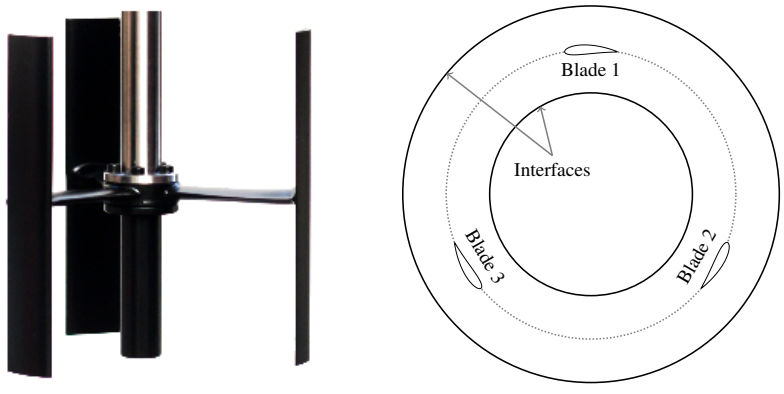

(a) (b)

Figure 1: Picture of the experimental turbine (a) and schematic of a horizontal section of the rotor showing the 3 blades and the boundaries (interfaces) with the two other sub-domains (b).

The experiments were run in a water tunnel with a width w $= 0.6$ m and a height $h = 0.55$ m. The blockage ratio is then $\epsilon = S/(\text{w} \times h) = 9.3\%$. The turbulence intensity at the turbine location was measured at 5.5% [2].

2.2 Numerical model

2.2.1 Mesh

The 2D computational domain is meshed with ICEM CFD, following a multi-block structured approach (Fig. 2) and is divided into three sub-domains (Fig. 1b):

- An outer sub-domain extending $15D$ upstream, $40D$ downstream and $30D$ on each side.
- A rotating ring containing the three blades and extending from $r = 0.7D$ to $r = 1.3D$, with r the radius from the turbine center. (102×10^3 cells)
- An inner sub-domain (with no shaft). (25×10^3 cells)

The boundaries of the outer domain are located away from the turbine to limit their effect on the solution as much as possible. The blockage ratio is here: $\epsilon = 1.7\%$, which is lower than the experimental value. It was deemed better to study a purely isolated turbine configuration considering that it would have been difficult to reproduce in two-dimensions the blockage ratio of the experiments (3D).

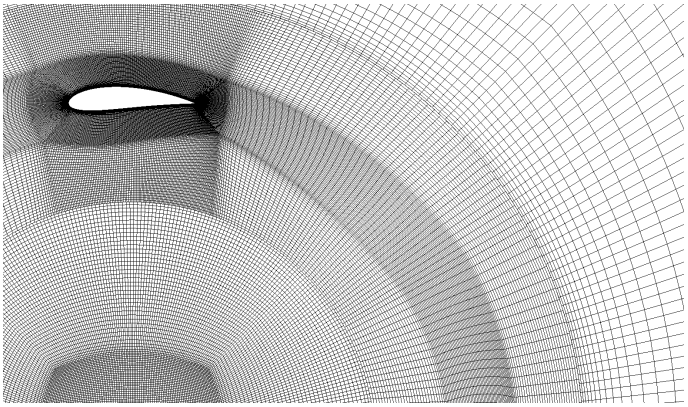

Figure 2: Close view of the mesh in the rotor region.

Each blade is represented by 314 mesh nodes and the size of the first row of cells, perpendicular to the blade surface, is 10^{-5} m at the leading edge and 3×10^{-5} m at the trailing edge so that $y^+_{max} < 5$ at any time during a revolution. A time step corresponding to a variation of the azimuthal angle of the turbine $\Delta\theta = 1^\circ$ is used in all cases. Although not shown here, the sensitivity to y^+ and time step have been studied at $TSR = 2$ and showed convergence for the values aforementioned. The computational domain size and the number of mesh nodes on each blade are beyond the recommended values [4, 5, 6].

To study the sensitivity of the turbine wake to mesh resolution, four outer sub-domain grids are tested (Tab. 1). The strategy adopted is to have a constant grid spacing ($\Delta x = \Delta y$) downstream of the turbine (Fig. 3) and until the outlet boundary. Therefore, within the O-grid surrounding the rotor sub-domain, the cells' size increases smoothly from the small cells observed in the rotor (Fig. 2) to the target cells' size described in Tab. 1. The region where this strategy is applied covers $4D$ in the y direction (Fig. 3). We made an exception to this method with the $D80$ grid for which the characteristics $\Delta x = \Delta y$ is

only valid until $20D$ downstream of the turbine. Further downstream, Δy remains the same but Δx is loosened in order to save cells.

Table 1: Details of the four mesh resolutions used for the outer domain.

Grid	$\Delta x = \Delta y =$ (m)	Number of cells ($\times 10^3$)
$D10$	$D/10 = 0.0175$	61
$D20$	$D/20 = 0.00875$	155
$D40$	$D/40 = 0.00438$	463
$D80$	$D/80 = 0.00219$	916

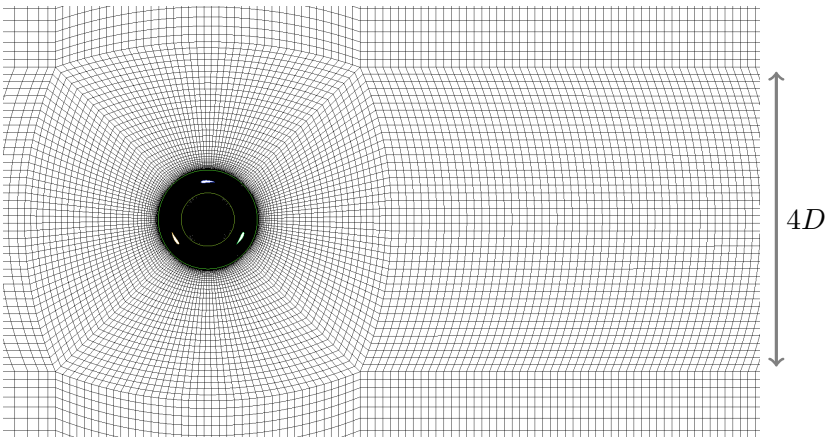

Figure 3: $D10$ mesh around the turbine and in the near wake. Water flows from left to right.

2.2.2 Turbulence model and numerical procedure

Incompressible Unsteady Reynolds-Averaged Navier-Stokes (URANS) equations are solved using OpenFOAM v1812. The k $-$ ω SST (Shear Stress Transport) turbulence model [7] is selected to model the Reynolds stresses. The numerical schemes used in the simulations are summarized in Tab. 2 and the pimpleFOAM solver is used with 20 iterations per time step. A case with 35 iterations per time step was run and showed no difference with the corresponding case using 20 iterations per time step.

A constant velocity $U_x = U_\infty = 2.3$ m/s is defined at the inlet boundary together with a turbulence intensity equal to 5% ($k = 0.0199$ m^2/s^{-2}). At the outlet boundary, a constant pressure $P = 0$ Pa is imposed. Blades are considered as *walls* with a *movingWallVelocity* type for U, a *zeroGradient* condition on the pressure, a *kqRWallFunction* on k and the *omegaWallFunction* on ω. Note that due to the fine mesh used close to the blades, the boundary layers are resolved and the wall function treatment is not used. The side boundaries of the outer domain are considered as *symmetryPlanes*. Finally, the interfaces between sub-domains are set as *cyclicAMI* boundaries.

Simulations with grids $D10$ to $D40$ are parallelized on 8 CPUs and require approximately one day to simulate 20 turbine revolutions (two days with $D40$). The simulation $D80$ is parallelized on 20 CPUs and requires approximately 20h to simulate 4 turbine revolutions. Simulations have been run for 80 turbine revolutions.

Table 2: Main numerical schemes used for every simulation in this study.

Term	Numerical scheme
ddtScheme	backward
gradScheme (k and ω)	cellLimited Gauss linear 1
gradScheme (others)	Gauss linear
divScheme (phi,U)	Gauss linearUpwindV grad(U)
divScheme (phi,k and ω)	Gauss limitedLinear 1
laplacianScheme	Gauss linear limited corrected 0.5
interpolationScheme	linear
snGradScheme	corrected

3 Results and discussion

3.1 Turbine performance

Before focusing on the turbine wake, we run simulations at $TSR = 1.5$, 2 and 2.5 with the grid $D20$ in order to compare the turbine performance (coefficient of power, $CP = \frac{C\Omega}{0.5\rho S U_\infty^3}$ and coefficient of thrust $C_T = \frac{F_x}{0.5\rho S U_\infty^2}$, with C the torque generated by the rotor, Ω the rotor rotational speed, and F_x the rotor thrust force) with experimental data [2]. Figure 4 shows that the URANS 2D simulations overpredict the coefficient of power but follow the same trend as the measurements. Especially, the best operating point is found to be $TSR = 2$ with both 2D simulations and experiments. The higher coefficients of power predicted by the 2D simulations can easily be explained by the absence of 3D effects like tip vortices, arm/blade junction losses and the interaction with the wake of the main shaft.

The simulations results shown in Fig. 4 are average values of CP and C_T calculated over the 10th revolution ($TSR = 1.5$) and over the 15th revolution ($TSR = 2$ and 2.5). The convergence criteria used in these cases was a decrease in the average coefficient of power by less than 1% between two consecutive revolutions. This convergence criteria is often used even though it is a little coarse. If those simulations had been run for a longer time (e.g. for 80 revolutions as in the next section), the coefficient of power would decrease further by a few percents.

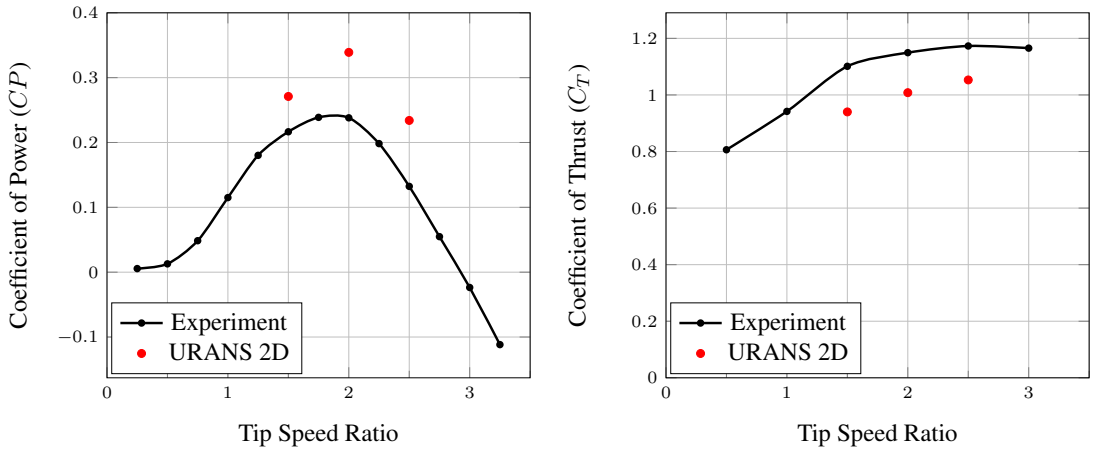

Figure 4: Comparison of measured and simulated coefficients of power (left) and coefficients of thrust (right).

Figure 4 (right) shows that the 2D simulations underpredict the thrust coefficient. Similar explanations as with the CP values can be made plus the fact that the thrust measured in the experiments includes a contribution from the arms and the shaft connecting the turbine blades to the generator. The arms and the shaft are not taken into account in the 2D simulations.

3.2 Mesh sensitivity of the turbine wake

This section focuses on the sensitivity of the simulation at $TSR = 2$ to the mesh resolution in the turbine wake. The four grids presented in Tab. 1 are used to this end.

Before looking at the wake, Tab. 3 shows that the resolution of the mesh in the outer sub-domain does not affect significantly the prediction of both CP and C_T after 80 rotor revolutions. Especially, grid $D20$ leads to only 0.5% and 0.3% increase in CP and C_T, respectively, compared to the finest grid tested, $D80$. It should be noted that when increasing the mesh resolution in the outer sub-domain, cells are refined both upstream and downstream of the rotor (Fig. 3). It is therefore difficult to determine whether the difference in CP and C_T comes from the better resolved wake or upstream flow.

Table 3: Coefficients of power (CP) and thrust (C_T) obtained with different grid resolutions in the turbine wake. Values are averaged over the 80th revolution.

Grid	CP	C_T
$D80$	0.299 (*Ref*)	0.948 (*Ref*)
$D40$	0.300 ($+0.1\%$)	0.949 ($+0.07\%$)
$D20$	0.301 ($+0.49\%$)	0.951 ($+0.28\%$)
$D10$	0.304 ($+1.56\%$)	0.956 ($+0.81\%$)

Figure 5 presents a qualitative analysis of the flow field in the near wake of the turbine (up to $6D$ downstream). Simulations using grids $D20$ to $D80$ show very similar flow patterns although the resolution of small flow structures (e.g. just downstream the turbine) improves with the number of cells. Grid $D10$ leads to a flow pattern in the near wake which is similar to the other grids. However, $6D$ downstream the turbine, where the wake seems to transition to a bluff-body regime, as described in [1], the grid $D10$ leads to a different behavior (or induces at least a phase shift in the wake oscillation).

A comparison of both average streamwise velocity and average turbulence kinetic energy profiles obtained with the grids $D10$, $D20$, $D40$ and $D80$ is presented in Fig. 6. To produce this figure, simulations have been run for 80 turbine revolutions and results averaged over the last 20 revolutions (60 to 80). In the far wake, 20 turbine revolutions correspond to 5 periods of velocity fluctuation (which corresponds to a Strouhal number $St = \frac{fD}{U_\infty} = 0.16$).

Fig. 6 shows that grids $D20$, $D40$ and $D80$ lead to almost exactly the same velocity profiles whatever the distance downstream the turbine. However, grid $D10$ leads to noticeable, even if still small, differences in the velocity profiles. This is especially true at $x = 8D$ where $D10$ predicts a slightly faster wake recovery than the other two grids.

The turbulence kinetic energy (k) profiles are a little more scattered than the velocity profiles. Especially at $x = 2D$, it is clear that the finer the mesh, the larger the peaks of k. Further downstream, $D20$, $D40$ and $D80$ curves superimpose almost perfectly while the $D10$ curves show some significant differences with the two others.

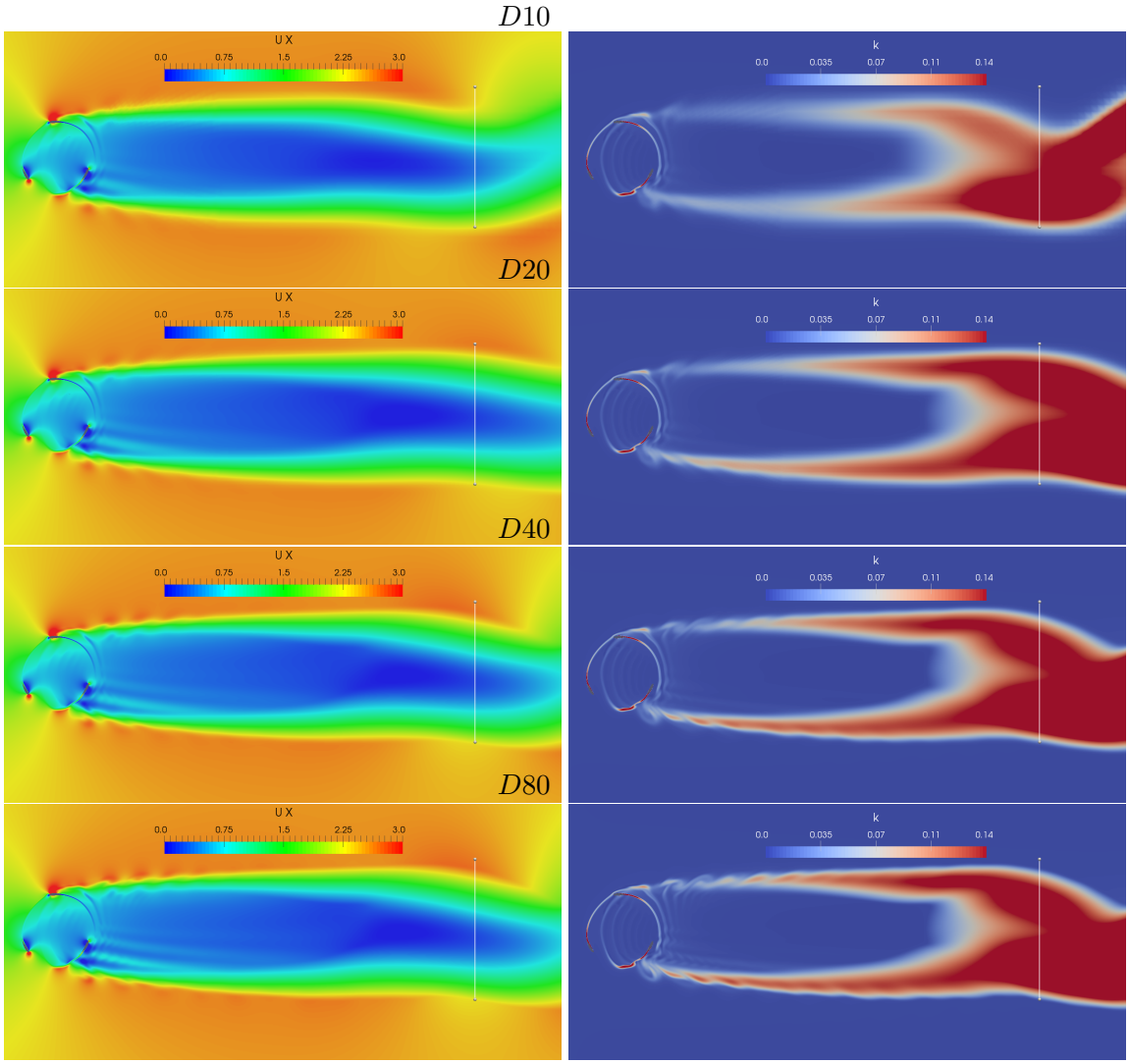

Figure 5: Instantaneous streamwise velocity (left) and turbulence kinetic energy (right) fields after 40 revolutions for grids $D10$ to $D80$. The line plotted on the right side of the figures is located at $x = 6D$.

The results presented in Tab. 3, Fig. 5 and Fig. 6 show that although the mesh resolution in the outer sub-domain does not affect significantly the turbine performance and the prediction of its wake, it is better to use a resolution equivalent to $\Delta x = \Delta y = D/20$ or finer in order to obtain a mesh insensitive solution. Lower mesh resolutions should be avoided.

3.3 Comparison to experimental data

In this section, we compare the simulation results obtained with grid $D40$ to measurements [2]. Figure 7a emphasizes the great difference between 2D simulations and actual 3D experiments. The 2D simulation predicts a wider wake at $x = 2D$ and significantly underpredicts the wake recovery from $x = 4D$ to $x = 12D$. The agreement between the 2D simulation and the measurements at $x = 12D$ is better than at lower x values but a 0.15 difference in non-dimensioned streamwise velocity remains.

Figure 7b shows that the 2D simulation underpredicts k at $x = 2D$ and $x = 4D$. The peak values are predicted further away from the turbine center than in the experiment. At $x = 6D$ and beyond, the 2D simulation significantly overpredicts k and the recovery is longer than in the experiment, as already observed on the streamwise velocity.

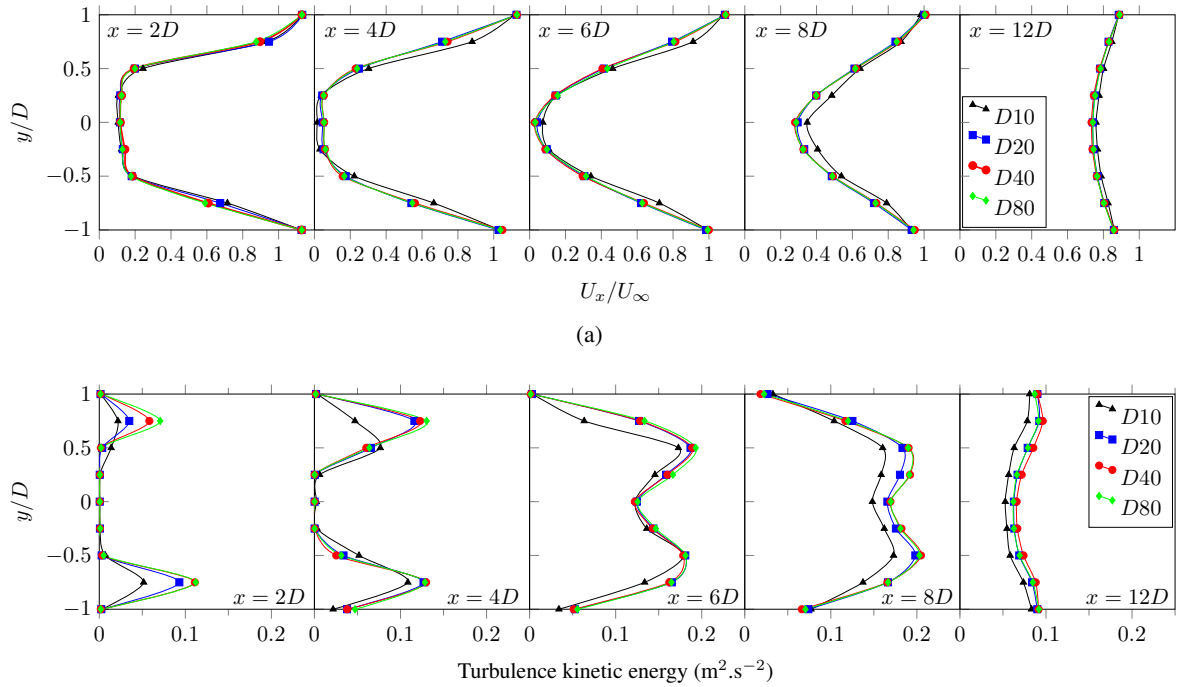

(a)

(b)

Figure 6: Comparison of non-dimensioned streamwise velocity profiles (a) and turbulence kinetic energy profiles (b) for grids $D10$, $D20$, $D40$ and $D80$ at five locations downstream of the turbine.

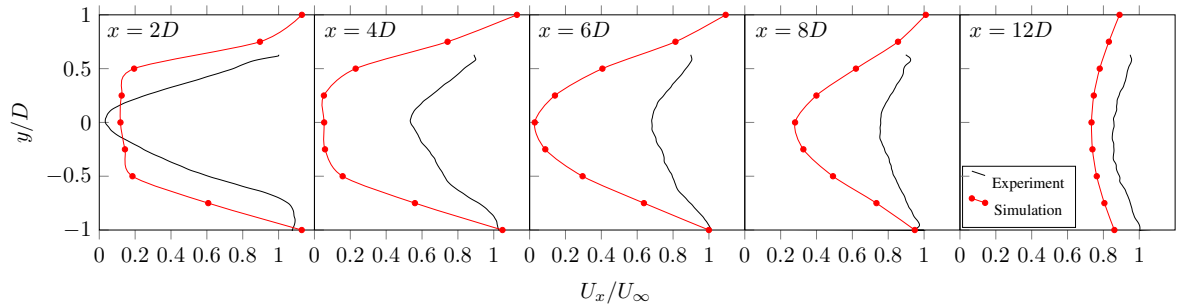

(a)

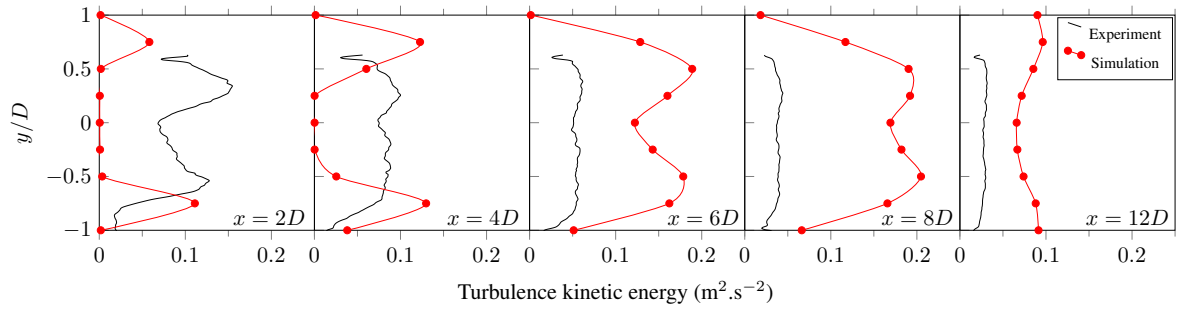

(b)

Figure 7: Comparison of measured and simulated (with grid $D40$) non-dimensioned streamwise velocity profiles (a) and turbulence kinetic energy profiles (b) at five locations downstream the turbine.

Note that due to the long distance between the upstream boundary and the turbine, the ambient turbulence intensity around the rotor is not 5% as set at the inlet. Instead, this value has decreased to almost 0.

This is explained by the absence of velocity gradient upstream of the turbine which results in only the destruction term to be active in the k equation of the turbulence model. This is not considered to have a significant effect on the turbine performance but it could affect the wake development and mixing. In particular, it can explain why the minimum value of k at $x = 2D$ is very close to zero. However, some studies have shown that the wake of a vertical axis turbine is not much affected by the ambient turbulence. Therefore, the main explanation for the differences observed in this work is assumed to be the 2D versus 3D approach.

4 Conclusions

2D URANS simulations of a vertical axis tidal turbine have been run with OpenFOAM using four grids with different mesh resolutions in the wake. The simulations have been compared between themselves in order to find the minimum mesh resolution in the wake above which further refinements do not improve significantly the solution. It was found that a mesh resolution equal to $\Delta x = \Delta y = D/20$ is enough to capture accurately the average velocity profiles in the wake of the turbine. This guideline, based on 2D simulations, is believed to be valid for 3D simulations as well.

The 2D simulation results have also been compared to already published experimental data [2]. The comparison gives valuable information about the differences between 2D simulations and 3D experiments and the consequences on the wake prediction. It was found that the 2D simulations significantly underpredict the wake recovery. This is of particular interest as it means that 2D simulations should not be used to study farms of high solidity turbines. 3D simulations using the same configuration as the one used in this study are planned in the near future to confirm this observation.

References

[1] D.B. Araya, T. Colonius, and J.O. Dabiri, Transition to bluff-body dynamics in the wake of vertical-axis wind turbines, Journal of Fluid Mechanics, 813 (2017) 346-381.

[2] V. Clary, T. Oudart, T. Maître et al., A simple 3D river/tidal turbine model for farm computation - Comparisson with experiments, Sixth International Conference on Estuaries and Coasts (ICEC), Caen, France (2018).

[3] H.F. Lam, H.Y. Peng, Study of wake characteristics of a vertical axis wind turbine by two- and three-dimensional computational fluid dynamics, Renewable Energy, 90 (2016) 386-398.

[4] A. Rezaeiha, I. Kalkman, B. Blocken, CFD simulation of a vertical axis wind turbine operating at a moderate tip speed ratio: Guidelines for minimum domain size and azimuthal increment, Renewable Energy, 107 (2017) 373-385.

[5] F. Balduzzi, A. Bianchini, R. Maleci, G. Ferrara, L. Ferrari, Critical issues in the CFD simulation of Darrieus wind turbines, Renewable Energy, 85 (2016) 419-435.

[6] T. Maître, E. Amet, C. Pellone, Modeling of the flow in a Darrieus water turbine: wall grid refinement analysis and comparison with experiments, Renewable Energy, 51 (2013) 497-512.

[7] F. Menter, Two-equation eddy-viscosity turbulence models for engineering applications, AIAA Journal, 32 (1994) 1598-1604.